Crystal Structures of HbA_2 and HbE and Modeling of Hemoglobin δ_4: Interpretation of the Thermal Stability and the Antisickling Effect of HbA_2 and Identification of the Ferrocyanide Binding Site in Hb‡

Udayaditya Sen,§ Jhimli Dasgupta,§ Debi Choudhury,§ Poppy Datta,|| Abhijit Chakrabarti,|| Sudipa Basu Chakrabarty,⊥ Amit Chakrabarty,⊥ and Jiban K. Dattagupta*,§

Crystallography and Molecular Biology Division, Saha Institute of Nuclear Physics, 1/AF Bidhan Nagar, Kolkata 700064, India, Biophysics Division, Saha Institute of Nuclear Physics, 37 Belgachia Road, Kolkata 700037, India, and Thalassemia Hospital, 19B Chetlahat Road, Kolkata 700027, India

Received May 28, 2004; Revised Manuscript Received July 23, 2004

ABSTRACT: Hemoglobin A_2 ($\alpha_2\delta_2$) is an important hemoglobin variant which is a minor component (2−3%) in the circulating red blood cells, and its elevated concentration in β-thalassemia is a useful clinical diagnostic. In β-thalassemia major, where there is β-chain production failure, HbA_2 acts as the predominant oxygen deliverer. HbA_2 has two more important features. (1) It is more resistant to thermal denaturation than HbA, and (2) it inhibits the polymerization of deoxy sickle hemoglobin (HbS). Hemoglobin E ($E26K^{\beta}$), formed as a result of the splice site mutation on exon 1 of the β-globin gene, is another important hemoglobin variant which is known to be unstable at high temperatures. Both heterozygous HbE (HbAE) and homozygous HbE (HbEE) are benign disorders, but when HbE combines with β-thalassemia, it causes E/β-thalassemia which has severe clinical consequences. In this paper, we present the crystal structures of HbA_2 and HbE at 2.20 and 1.74 Å resolution, respectively, in their R2 states, which have been used here to provide the probable explanations of the thermal stability and instability of HbA_2 and HbE. Using the coordinates of R2 state HbA_2, we modeled the structure of T state HbA_2 which allowed us to address the structural basis of the antisickling property of HbA_2. Using the coordinates of the δ-chain of HbA_2 (R2 state), we also modeled the structure of hemoglobin homotetramer δ_4 that occurs in the case of rare HbH disease. From the differences in intersubunit contacts among β_4, γ_4, and δ_4, we formed a hypothesis regarding the possible tetramerization pathway of δ_4. The crystal structure of a ferrocyanide-bound HbA_2 at 1.88 Å resolution is also presented here, which throws light on the location and the mode of binding of ferrocyanide anion with hemoglobin, predominantly using the residues involved in DPG binding. The pH dependence of ferrocyanide binding with hemoglobin has also been investigated.

Mammalian hemoglobins function as heterotetramers comprising two α-type and two β-type globin chains. During development from embryo to adult, the genes specific for globin chains are switched on and off, accounting for the different hemoglobin types. Hemoglobin A_2 is a naturally occurring hemoglobin variant, which is expressed at a low concentration (∼2−3%) in normal individuals but at a high level (∼3.5−7% for minor and >15% for major) in patients having β-thalassemia, for whom it is used as a diagnostic. In β-thalassemia, a small deletion at the 5′ portion of the β-globin gene removes the promoter but stops 3′ to the δ-globin gene in chromosome 11 (*1*), causing a β-chain production failure. The production of the α-chain, however, continues at a near-normal rate, which stimulates the production of δ- and γ-chains. δ- and γ-chains thus expressed combine with the α-chains to increase the level of hemoglobin A_2 (HbA_2, $\alpha_2\delta_2$) and hemoglobin F (HbF, $\alpha_2\gamma_2$).

Table 1: Differences in the Amino Acid Sequence between β- and δ-Chains in Human Hemoglobin

residue	β-subunit	δ-subunit	residue	β-subunit	δ-subunit
9	Ser	Thr	87	Thr	Gln
12	Thr	Asn	116	His	Arg
22	Glu	Ala	117	His	Asn
50	Thr	Ser	125	Pro	Gln
86	Ala	Ser	126	Val	Met

The oxygen binding property of HbA_2 was a matter of dispute (*2*, *3*), but it has been shown that the recombinant HbA_2 has a higher oxygen affinity than HbA and its response to the allosteric regulators such as 2,3-diphosphoglycerate (DPG)[1] is weaker than the corresponding properties for the adult hemoglobins (*4*). The δ-chain of HbA_2 differs from the β-chain of adult hemoglobin (HbA, $\alpha_2\beta_2$) at 10 sites (*5*) in the amino acid sequence (Table 1). From the thermal denaturation experiments, Perutz and Raidt (*6*) reported that

‡ The coordinates of HbE, HbA_2, and HbA_2^{FC} have been submitted to the RCSB as entries 1NQP, 1SI4, and 1SHR, respectively.

* To whom correspondence should be addressed. Telephone: +91-033-2321-4986. Fax: +91-033-2337-4637. E-mail: jiban@cmb2.saha.ernet.in.

§ Crystallography and Molecular Biology Division, Saha Institute of Nuclear Physics.

|| Biophysics Division, Saha Institute of Nuclear Physics.

⊥ Thalassemia Hospital.

[1] Abbreviations: Hb, hemoglobin; HbA_2^{FC}, ferrocyanide-bound hemoglobin A_2; HbS, sickle hemoglobin; DPG, 2,3-diphosphoglycerate; CVFF, consistent valence force field.

10.1021/bi048903i CCC: $27.50
Published on Web 09/11/2004

HbA_2 is more resistant to thermal denaturation than HbA because of an additional contact at the $\alpha_1\delta_1$ interface, due to the $His116^{\beta} \rightarrow Arg116^{\delta}$ mutation. NMR studies also indicated that the replacement of β-chains with δ-chains in HbA_2 slightly perturbs the $\alpha_1\delta_1$ interface (*5*). Besides this, HbA_2 can inhibit the polymerization of deoxy sickle hemoglobin (HbS) *in vitro*, indicated by a marked increase in the minimum gelling concentration (MGC) values for the HbS/HbA_2 mixture (41.0 g/dL) over those for HbS/HbA mixtures (32.2 g/dL) (*7*). Several studies, including NMR (*5*) and studies of minimum gel concentration with naturally occurring hemoglobin variants, like Lepore hemoglobins (*7*), along with site-directed mutagenesis experiments (*8*) indicated that $Gln87^{\delta}$ and $Ala22^{\delta}$ are the potential sites for the inhibition of polymerization of deoxy HbS, but the structural basis of its antisickling property has not yet been established.

Hemoglobin E [HbE; Glu26(B8) → Lys], a result of splice site mutation (GAG → AAG) in exon 1 of the β-globin gene (*9*, *10*), is the most common hemoglobin variant, most prevalent in Southeast Asia (*11*, *12*). Geographic overlap in the distributions of *Plasmodium falciparum* and hemoglobin E indicates that this hemoglobinopathy protects individuals against malarial infection (*13*). Both heterozygous HbE (HbAE) and homozygous HbE (HbEE) conditions are asymptomatic (minimally anemic with microcytic and hypochromic red blood cells). However, HbE combined with β-thalassemia causes E/β-thalassemia having severe clinical consequences. Thermal denaturation experiments performed on blood from E/β-thalassemics in the temperature range of 39−41 °C showed the instability of HbE, a finding that was also observed in homozygous HbE (*14*). Pscheidt *et al*. (*15*) also showed the instability of HbE by performing a heat test at 50−60 °C, and they suggested that, in particular, any change that reduces the contacts between the subunits that compose the hemoglobin would generate its instability.

In this paper, we present the crystal structures of HbA_2 and HbE in cyanomet form in the R2 state. The three-dimensional structures of HbA_2 and HbE allow us to provide the probable explanations for the thermal stability of HbA_2 and the instability of HbE, from the structural point of view. To understand the antisickling property of HbA_2, a phenomenon that occurs in the deoxy state, we modeled the structure of T state HbA_2, from the crystal structure of R2 state HbA_2. This model has been used here to provide the probable structural basis of its antisickling property, especially the role of $Gln87^{\delta}$ at the atomic level. Moreover, the structure of HbA_2 provides the atomic details of the hemoglobin δ-chain for the first time, which we have used to model the structure of homotetrameric hemoglobin δ_4, a consequence of rare HbH disease that occurs in α-thalassemia in adulthood. Comparison of the intersubunit contacts of δ_4 with β_4 and γ_4 helped us to form a hypothesis about the possible tetramerization pathway of δ_4. It is known that ferrocyanide anion, produced during the oxidation of heme iron using ferricyanide, binds with hemoglobin probably at the DPG binding site (*16*, *17*). A high-resolution crystal structure of ferrocyanide-bound HbA_2 is presented here, which throws light on the location and the mode of binding of ferrocyanide anion with hemoglobin. The influence of pH on the binding of ferrocyanide with hemoglobin is also investigated and the results support the structural observations.

MATERIALS AND METHODS

Purification, Crystallization, and Data Collection. HbA_2 and HbE were purified from the blood samples of thalassemic patients, taken for diagnosis to Thalassemia Hospital, using cation exchange column chromatography, as elaborated in our previous work (*18*). HbE was purified from the E/β-thalassemic blood samples containing a high level of HbE, whereas HbA_2 was purified from the blood samples of β-thalassemia minor patients. All the hemoglobin samples were characterized by the Bio-Rad Variant (*19*).

Both HbE and HbA_2 were purified in cyanomet form by adding an equimolar amount of $K_3[Fe(CN)_6]$ and protein, in the presence of KCN. During this process, in one batch of the preparation, we purified a ferrocyanide-bound form of HbA_2 (hereafter termed HbA_2^{FC}) in an effort to understand the location and mode of binding of ferrocynide anion with hemoglobin. HbE and HbA_2^{FC} were crystallized in space groups $P2_12_12_1$ and $P2_1$, respectively, using polyethylene glycol (PEG) as a precipitant. Crystallizations and data collections of HbE and HbA_2^{FC} up to 1.73 and 2.1 Å resolution were reported by us previously (*18*). Later, the diffraction data of HbA_2^{FC} were collected up to 1.88 Å resolution (Table 2).

In contrast to HbA_2^{FC}, HbA_2 crystallizes in orthorhombic space group $P2_12_12_1$ (using Crystal Screen Cryo #22 of Hampton Research) with one Hb tetramer in the asymmetric unit and the following unit cell parameters: $a = 60.45$ Å, $b = 88.19$ Å, and $c = 104.59$ Å. Crystals, grown in the presence of a cryoprotectant, were immediately flash-frozen in a stream of nitrogen (Oxford cryo-system) at 100 K, and X-ray diffraction data were collected up to 2.2 Å, using a 30 cm MAR research image-plate detector. The data were processed using DENZO and SCALEPACK from the HKL program package (*20*). A total of 28 343 reflections were collected with an R_{merge} of 6.9% and an overall completeness of 97.7% (Table 2).

Structure Determination and Refinement. Molecular replacement calculations for HbA_2^{FC} and HbE were carried out using AMoRe (CCP4) (*21*) with the data between 10 and 3.5 Å. No clear solution was obtained using either the model of human deoxy HbA in the T state (PDB entry 2HHB) (*22*) or the model of liganded human HbA in the R state (PDB entry 1HHO) (*23*). However, the coordinates of liganded human carbonmonoxy adult Hb tetramer in the R2 state (PDB entry 1BBB) (*24*) gave a single unambiguous solution for both HbA_2^{FC} and HbE. Side chains of 11 residues of each β-chain (10 residues that differed between β and δ and the single amino acid, $Glu26^{\beta}$, of HbE) were truncated to Ala in the starting model. For the R_{free} calculation (*25*), in each case, 5% of the reflections were selected randomly. O (*26*) and CNS (*27*) were used for model building and refinement, respectively.

The solution for HbA_2^{FC} was obtained with a correlation coefficient of 64.5% and an *R*-factor of 37.1%. Subsequent rigid body refinement, treating each globin chain as a separate rigid body, further reduced the *R*-factor to 33.1% (R_{free} = 35.2%). Electron density maps, calculated using the coordinates of rigid body refinement, showed clear side chain densities for the 10 residues of each δ-chain that differ from those of the β-chain, whereas the electron density of the 26th residue fit with Glu. All these residues were replaced by the

Table 2: Data Collection and Refinement Statistics of HbA_2, HbE, and HbA_2^{FC}

	HbA_2[a]	HbE[a]	HbA_2^{FC}[a]
	Data Collection		
space group	$P2_12_12_1$	$P2_12_12_1$	$P2_1$
unit cell	$a = 60.45$ Å, $b = 88.19$ Å, $c = 104.59$ Å	$a = 60.89$ Å, $b = 95.81$ Å, $c = 99.08$ Å	$a = 54.45$ Å, $b = 83.99$ Å, $c = 62.69$ Å, $\beta = 99.86°$
no. of Hb tetramers in the asymmetric unit	1	1	1
resolution range (Å)	15−2.20 (2.2−2.28)	15−1.74 (1.74−1.82)	15−1.88 (1.88−2)
completeness (%)	97.7 (99.4)	97.5 (91.1)	98.6 (99.4)
R_{merge} (%)	6.9 (27.3)	5.3 (41.2)	5.4 (34.8)
mosaicity	0.69	0.47	0.63
average redundancy	2.5	3.3	2.6
average I/σ	9.8 (2.3)	19.9 (2.4)	16.1 (2.8)
	Refinement		
R_{cryst} (%)	21.8 (31.6)	18.7 (31.0)	16.7 (31.7)
R_{free} (%)[b]	25.9 (34.5)	20.7 (32.5)	19.5 (35.6)
no. of heme atoms	176	176	176
no. of non-heme atoms (protein/water)	4372/667	4357/771	4388/752
no. of ligand atoms attached with heme iron	8	8	8
rmsd[c] for bond lengths (Å)	0.008	0.006	0.005
rmsd for bond angles (deg)	1.25	1.18	1.09
$\langle B \rangle$ (Å^2)			
protein	33.88	23.10	19.26
water	39.38	37.58	34.98
heme groups	39.06	23.50	18.04
Ramachandran plot (%)[d]			
most favored	90.4	92.4	92.6
allowed	9.6	7.6	7.4
disallowed	0.0	0.0	0.0

[a] Values in parentheses correspond to the outermost resolution shell. [b] $R_{cryst} = \sum_{hkl}||F_o| - |F_c||/\sum_{hkl}|F_o|$; 5% of the reflections were excluded for the R_{free} calculation. [c] rmsd is the root-mean-square deviation. [d] Analyzed by PROCHECK (*33*).

actual δ-chain residues, and cycles of model rebuilding and refinement further reduced the *R*-factor to 26.3% (R_{free} = 29.8%). A composite OMIT map was calculated at this stage which indicated that the C-terminal part of one of the δ-chains acquires a somewhat extended conformation, compared to the usual helical one, and comes close to the C-terminal part of the other δ-chain. On the other hand, three strong ($\sim 15\sigma$) positive peaks were observed in the $F_o - F_c$ map near the histidyl residues of the C-terminal part of the δ-chains which were assigned as iron atoms, based on their coordination distances from the neighboring residues and as ferricyanide was added during sample preparation. Subsequent conjugate gradient minimization, *B*-factor refinement, and water picking refinement reduced the *R*-factor to 16.7% (R_{free} = 19.5%) for the data between 15 and 1.88 Å.

The structure of HbA_2 was determined by molecular replacement using the refined coordinates of HbA_2^{FC} as a search model. The last five residues of each δ-chain, the three iron (non-heme) atoms that came from ferrocyanide, and their attached ligands were removed from the starting model. One molecule of HbA_2 in the R2 state was found in the asymmetric unit with a correlation coefficient of 72.1% and an *R*-factor of 38.5%. The structure was refined by cycles of manual model rebuilding and refinement to an *R*-factor of 21.8% (R_{free} = 26.4%).

For HbE, the solution was obtained with a correlation coefficient of 73.1% and an *R*-factor of 33.5%, which upon rigid body refinement further reduced the *R*-factor to 31.1% (R_{free} = 32.2%). A composite OMIT map was calculated at this stage which showed electron density for the side chain of Lys26$^{\beta}$ unequivocally and the 10 other residues which were kept as Ala, matched with HbA. The structure was refined by a few cycles of model building and refinement to an *R*-factor of 24.5% (R_{free} = 26.3%). Progressive inclusion of water molecules and cyanide ions followed by individual *B*-factor refinement reduced the *R*-factor to 18.7% (R_{free} = 20.8%). The data collection and refinement statistics for the three structures are given in Table 2.

Molecular Modeling of T State HbA_2. To model the T state structure of HbA_2 from the coordinates of cyanomet HbA_2, we have used the coordinates of human deoxyhemoglobin (PDB entry 3HHB) as a template, accounting for the structural changes that occur during the T → R (R2) transition. Crystallographic studies have established that the T and R states are structurally distinct (*28*), differing in their quaternary structures by a relatively simple movement of the $\alpha_1\beta_1$ and $\alpha_2\beta_2$ dimers (*29*). Moreover, during the T → R transition, the heme iron moves toward the porphyrin plane and pulls the proximal histidine (F8). This movement shifts the F helix, the EF corner, and the FG corner which in turn causes the rupture of salt bridges at the $\alpha_1\beta_2$ and $\alpha_2\beta_1$ interfaces.

To model T state HbA_2, $\alpha_1\delta_1$ and $\alpha_2\delta_2$ dimers of HbA_2 were superposed on the corresponding dimers of 3HHB with rmsds of 0.71 and 0.65 Å, respectively. The EF corner, the F helix, the FG corner, and the three carboxy-terminal residues were not taken in this superposition scheme. Later, the excluded portions were superposed on the corresponding sites of 3HHB with an average rmsd of ~0.7 Å. The superposed coordinates were then appended appropriately, and the resulting coordinates of the model were energy minimized using the DISCOVER-3 module of InsightII from Molecular Simulations Inc. (MSI, San Diego, CA). To start, hydrogen atoms were generated at pH 7.0 and potentials were assigned using the CVFF force field with a distance-independent dielectric constant of 4.0. The generated hydrogen atoms were then minimized keeping all the heavy atoms fixed. No cross-terms were used in the energy

expressions. Nonbonded interactions were evaluated using an atom-based method with a cutoff distance of 9.5 Å. The protein was solvated, by a water shell of 10 Å capping, using the SOAK utility of the DISCOVER-3 module. Generated water molecules were energy minimized (steepest descent followed by conjugate gradient), and then the protein water assembly was minimized using the steepest descent algorithm (down to a gradient of <100 kcal mol^{-1} Å^{-1}) followed by conjugate gradient minimization (down to <10 kcal mol^{-1} Å^{-1} and then to 0.01 kcal mol^{-1} Å^{-1}) successively.

Modeling of δ_4. High-resolution crystal structures of β-type homotetramers such as β_4 (*30*, *31*) and γ_4 (*32*) are available in the Protein Data Bank. The structures of liganded β_4 homotetramer (*30*) and Hb Barts γ_4 (*32*) essentially share the same quaternary structure; the whole γ_4 tetramer can be superposed on β_4 with an rms difference of only 0.9 Å. On the basis of this, Kidd *et al*. concluded that all β-type homotetramers have the same characteristic quaternary structures which are unaffected by the sequence differences in the individual subunit. Since the δ-globin chain differs from the β-chain at only 10 sites, compared to the difference of δ with γ at 42 sites, the crystal structure of CO-β_4 (PDB entry 1CBM) was used as a template to model the structure of δ_4. The δ-chain, obtained from the crystal structure of HbA_2, was individually superposed on each β-chain of β_4 on the basis of their main chain atoms. In CO-β_4, Arg40 and Asp99 of both subunits, which cluster together at the $\beta_1\beta_4$ ($\alpha_1\beta_2$) interface, can form altogether two salt bridges, but the steric conflict prevents the simultaneous formation of both the salt bridges. Hence, in the δ_4 model, only one pair (Arg40 and Asp99) was modeled as an intersubunit salt bridge. Cys112 of both chains was modeled in antiposition as seen in the crystal structure of CO-β_4. The resulting δ_4 structure was solvated and energy minimized using the DISCOVER-3 module of InsightII, following the procedure indicated in the previous section, down to 0.01 kcal mol^{-1} Å^{-1} using the steepest descent and conjugate gradient algorithm.

pH-Dependent Studies on Ferrocyanide Binding with HbA. Purified normal adult HbA samples in 10 mM phosphate buffer (pH 6.7) containing 100 mM NaCl were used to study the influence of pH on ferrocyanide binding with hemoglobin. Hb samples (2 mL) were taken in each case from this stock, and the pH dependence of binding of ferrocyanide to hemoglobin was monitored. The buffer of the protein solutions was exchanged exhaustively against the buffers at pH 5.5, 6.2, and 8.5 using the Amicon filter units with a 30 kDa cutoff to ensure equilibrium at that particular pH. The buffers, used for these studies, were 50 mM sodium cacodylate (pH 5.5 and 6.2) and 50 mM Tris-HCl (pH 8.5). An equimolar amount of ferricyanide was added to all three protein samples, and the mixtures were incubated at room temperature for 2 h (reaction volume maintained at 300 μL in each case). Ferric hemoglobin was separated from excess ferri/ferrocyanide using a Sephadex G-25 column (1 cm $\times$ 15 cm) preequilibrated with the respective buffer. Fractions containing hemoglobin were pooled, and UV−vis spectra were recorded using a Unicam UV 540 UV−vis absorption spectrophotometer. HbA_2^{FC} crystals were also dissolved in 50 mM Tris-HCl (pH 8.5), and the spectrum was recorded as described above.

RESULTS AND DISCUSSION

The crystal structures of HbA_2, HbE, and HbA_2^{FC} refined well, and they exhibit good stereochemistry. The $2F_o - F_c$ map for the entire polypeptide chain, in each case, is excellent and shows well-defined electron densities for all the mutations in the δ-chains of HbA_2 and HbA_2^{FC} as well as for Lys26$^{\beta}$ of HbE. Ramachandran plots of main chain torsion angles (ϕ and φ), calculated using the refined coordinates of HbA_2, HbA_2^{FC}, and HbE with PROCHECK (*33*), show that 90.4, 92.6, and 92.4% of the residues, respectively, lie in the most favored region with no residue in the disallowed regions.

The overall molecular structure of HbA_2 is similar to that of HbA in the R2 state (PDB entry 1BBB) (*19*) with slight subunit motions. The $\alpha\delta$ dimer of HbA_2 is superposed on the $\alpha\beta$ dimer of HbA with an rms deviation of 0.41 Å, whereas this value is 0.55 Å when all the four chains are superposed. When the α-chains are superposed individually, the rmsd value is 0.38 Å and the corresponding value for the β/δ-chain is 0.31 Å. The structures of HbA_2^{FC} and HbA_2 are very similar, differing only at the site of ferrocyanide binding near the C-terminus of δ-chains.

Structural Changes at the Mutation Sites of HbA_2 and Its Thermal Stability. Although the overall structure of HbA_2 is similar to that of HbA, changes are observed at certain sites of the δ-chain where it differs from the β-chain (residues 4−17, 20−26, and 116−127) in amino acid sequence along with residues 71−76. When all 146 C_α atoms of the δ-chain were superposed on the β-chain, the rms deviation was 0.31 Å, whereas the value was 0.22 Å when the aforementioned regions were excluded from the superposition scheme. In the latter superposition, helix A of the δ-chain was observed to be displaced by 0.8 Å, away from the H helix (Figure 1). In an earlier modeling study (*4*), Inagaki *et al*. speculated that the Val126$^{\beta}$ → Met126$^{\delta}$ mutation would generate unfavorable contacts with Leu14$^{\delta}$ of helix A, resulting in a weakening of both the stabilizing interactions (Val11$^{\delta}$ O•• •Tyr130$^{\delta}$ OH and the salt bridge between Lys17$^{\delta}$ and Glu121$^{\delta}$). In the crystal structure of HbA_2, we find that the side chain SD atom of Met126$^{\delta}$, instead of facing Leu14$^{\delta}$, points toward the peptide bond between Ala10$^{\delta}$ and Val11$^{\delta}$ (Figure 1), causing the shift of helix A, which in turn slightly shifts the neighboring portion of the E helix (residues 71$^{\delta}$−76$^{\delta}$). The aforementioned stabilizing interactions, however, remain intact in the crystal structure of HbA_2.

Glu26$^{\beta}$ of HbA is an important residue near the $\alpha_1\beta_1$ interface, which forms hydrogen bonds with Arg30$^{\beta}$ of helix B and His117$^{\beta}$ of helix G and compensates for the local accumulation of positive charge. In HbA_2, the mutation of His117$^{\beta}$ to Asn$^{\delta}$, a residue with a smaller side chain, allows Glu26$^{\delta}$ to reorient itself where it comes close to Asn117$^{\delta}$ and maximize the total number of hydrogen bonds (Figure 2a). In this new orientation, Glu26$^{\delta}$ can still maintain the hydrogen bond with Arg30$^{\delta}$, and in addition to that, it can form four hydrogen bonds with residues Arg116$^{\delta}$ and Asn117$^{\delta}$: Glu26$^{\delta}$ OE1 forms hydrogen bonds with Arg116 NH2 and Asn117 ND2, whereas Glu26$^{\delta}$ OE2 forms hydrogen bonds with Arg116 NE and Arg116 NH2. The extra interactions observed between helices B and G of HbA_2 would not have been possible if the side chain of Glu26$^{\delta}$ was oriented like HbA.

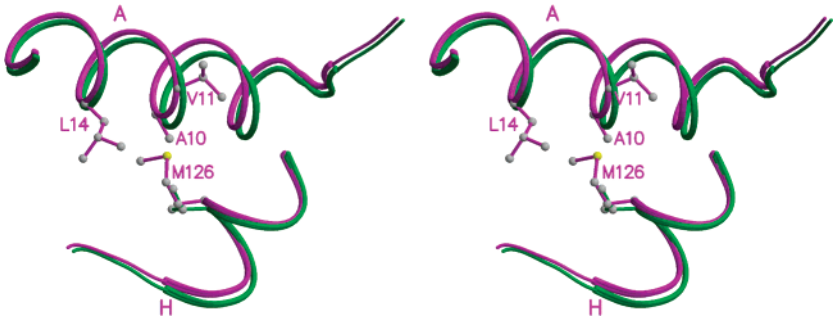

FIGURE 1: Stereoscopic representation of the superposition of helices A and H of the HbA_2 δ-chain (magenta) on the HbA β-chain (green). The figure shows a shift of helix A away from helix H in the case of HbA_2. The helices are shown as thin ribbons, and residues Ala10, Val11, Leu14, and Met126 of the δ-chain are shown in ball-and-stick form. This figure was generated with MOLSCRIPT (*57*) and RASTER3D (*58*).

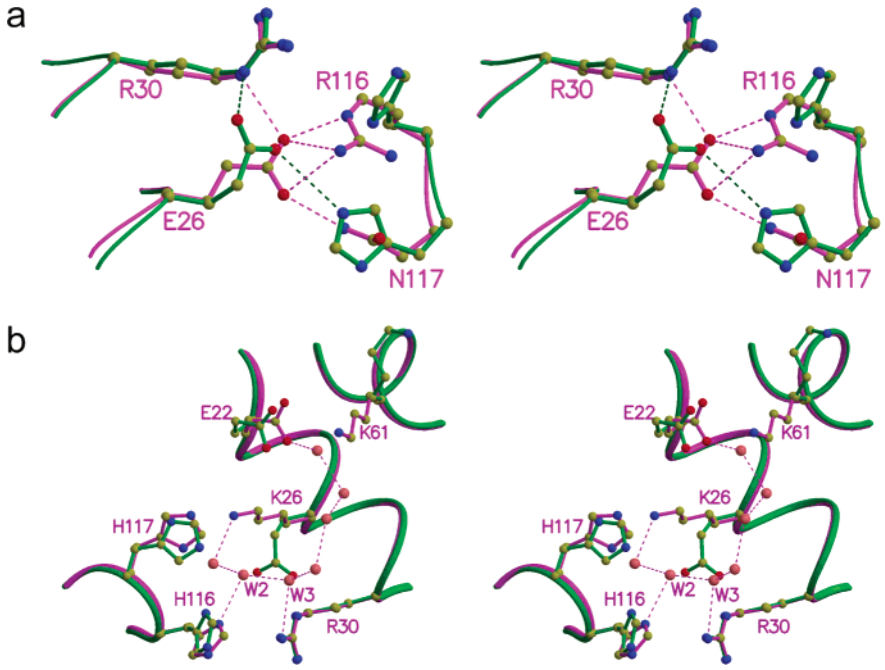

FIGURE 2: (a) Stereoscopic representation of the hydrogen bonding interactions between $Glu26^{\delta/\beta}$ and $Arg30^{\delta}$, $Arg116^{\delta}$, and $Asn117^{\delta}$ of HbA_2 (magenta) and $Arg30^{\beta}$, $His116^{\beta}$, and $His117^{\beta}$ of HbA (green). The number of hydrogen bonds (dashed lines, same color code) made by $Glu26^{\delta/\beta}$ is greater in HbA_2 than in HbA. (b) Stereoscopic representation of the structural changes around $Lys26^{\beta E}$. Side chains of HbE (magenta) that are structurally different from HbA (green) are shown in ball-and-stick form and labeled. The water molecules (pink balls), which form a network in HbE, are connected by hydrogen bonds (dashed lines). This figure was generated with MOLSCRIPT (*57*) and RASTER3D (*58*).

The involvement of helices B, G, and H of the β-chain in the intersubunit contact at the $\alpha_1\beta_1$ (or $\alpha_2\beta_2$) interface is well-known. From the thermal denaturation studies on HbA_2, Perutz *et al.* (*6*) speculated that two of the 10 substitutions in the δ-chain, belonging to helices G and H, are responsible for the extra thermal stability of HbA_2: $Arg(G18)116^{\delta}$ making an extra hydrogen bond at the $\alpha_1\delta_1$ interface and $Met(H4)126^{\delta}$ making intrasubunit nonpolar contacts with $Val11^{\delta}$ of helix A. In HbA, $His(G18)116^{\beta}$ forms a hydrogen bond with the carbonyl O of $Pro114^{\alpha}$ at the $\alpha_1\beta_1$ interface but is not involved in any intrasubunit hydrogen bonding with $Glu(B8)26^{\beta}$. In the crystal structure of HbA_2, we have seen that $Glu(B8)26^{\delta}$ forms three intrasubunit hydrogen bonds with NE and NH2 atoms of $Arg(G18)116^{\delta}$ (Figure 2a), leaving only the NH1 atom for intersubunit contact with the carbonyl O of Ala14 of α_1, thereby ruling out the possibility of the formation of extra hydrogen bonds at the $\alpha_1\delta_1$ interface. On the other hand, $Met(H4)126^{\delta}$ forms a number of nonpolar contacts with the backbone and side chain atoms of $Ala10^{\delta}$ as well as with the main chain N atom of $Val11^{\delta}$ of helix A, instead of $Val11^{\delta}$ alone, as suggested previously (*6*). Although we do not see the possibility of an extra intersubunit hydrogen bond at the $\alpha_1\delta_1$ interface, the additional salt bridge interactions among the residues of helices B and G (shown in Figure 2a) and the nonpolar contacts formed between helices A and H probably contribute to the extra thermal stability of HbA_2. It should be noted that the ΔG of thermal stabilization of HbA_2 is 1.2 kcal M^{-1} more than that of HbA at 45 °C and 3 kcal M^{-1} more than that at 57 °C (34).

The intersubunit contact area, calculated by GRASP (Table 3), for HbA_2 and HbA (PDB entry 1BBB) shows that the $\alpha_1\delta_1$ inetrface of HbA_2 (1759 Å^2) is similar to the $\alpha_1\beta_1$ (or $\alpha_2\beta_2$) interface of HbA (1765 Å^2), whereas the $\alpha_1\delta_2$ (or $\alpha_2\delta_1$) interface of HbA_2 (912 Å^2) is slightly larger compared to the corresponding interface of HbA (850 Å^2). Comparison

Table 3: Comparison of the Contacting Areas (Å^2) of Subunit Interfaces for HbA and HbA_2

	HbA	HbA_2		HbA	HbA_2
$\alpha_1\beta_1$ ($\alpha_1\delta_1$) interface	1765	1759	$\alpha_1\beta_2$ ($\alpha_1\delta_2$) interface	850	912
$\alpha_1\alpha_2$ interface	772	796	$\beta_1\beta_2$ ($\delta_1\delta_2$) interface	316	325

of inetrsubunit contacts (calculated using CONTACT from the CCP4 suite) also shows that an additional hydrogen bond appears at the $\alpha_1\delta_2$ (or $\alpha_2\delta_1$) interface between Asp94$^{\alpha 1}$ OD2 and Trp37$^{\delta 2}$ NE1 in HbA_2. These two facts together indicate a slightly more stable R2 state of HbA_2 than HbA which when coupled with its decreased level of DPG binding, as observed by Inagaki *et al*. (*4*), provides a plausible reason for the slight increase of the oxygen affinity of HbA_2.

Role of the Glu26$^\beta$ → Lys Mutation in the Structure of HbE. As expected, the overall structure of HbE is similar to the structure of HbA (R2 state). The $\alpha\beta$ dimer of HbE can be superposed on that of HbA (PDB entry 1BBB) with an rms deviation of 0.26 Å (for 287 C_α atoms), whereas the value is 0.37 Å when the tetramers (574 C_α atoms) are superposed. However, there are some local side chain alterations due to the loss of the salt bridge interaction at the E26K$^\beta$ mutation site. As stated earlier, the Glu26$^\beta$ side chain of HbA interacts with His117$^\beta$ and Arg30$^\beta$, whereas in HbA_2, Glu26$^\delta$, apart from maintaining the interactions described above, makes three extra hydrogen bonds with Arg116$^\delta$ of helix G. In HbE, the 26th residue is mutated to Lys, which can no longer face His117$^\beta$ and Arg30$^\beta$ due to steric and/or charge repulsion and points toward the surface (Figure 2b). As a result, the side chains of His116$^\beta$, His117$^\beta$, Met55$^\beta$, Lys61$^\beta$, and Glu22$^\beta$, immediately surrounding the mutation site, slightly reorient themselves, but the side chain orientation of Arg30$^\beta$ remains unchanged (Figure 2b). Interestingly, a network of water molecules is found here (W1−W7, counting counterclockwise from Lys26$^\beta$ to Glu22$^\beta$ in Figure 2b) which extends from Lys26$^\beta$ to Glu22$^\beta$. Two of these water molecules, W2 and W3, are buried and correspond with the positions of the OE1 and OE2 atoms of Glu26$^\beta$, respectively. The side chain of His116$^\beta$ rotates in HbE so that its ND1 atom forms a hydrogen bond with W2, but the NE2 atom remains in a position to maintain the intersubunit contact with the carbonyl O of Ala14$^\alpha$. The other buried water molecule, W3, forms a hydrogen bond with the NH2 atom of Arg30. Due to the loss of the hydrogen bond with the 26th residue, the side chain of His117$^\beta$ flips and its NE2 atom now interacts with another water molecule (not shown in the figure). Previous studies on hemoglobin instabilities suggest that HbE can be unstable when subjected to an increase in temperature (*14*, *15*). Our structural studies show that, although there is no direct hydrogen bond between helices B and G near the mutation site of HbE (Figure 2b), the intersubunit contacts remain the same as those of HbA, presumably due to the presence of the water network that partially connects helices B and G. Among these water molecules, only W2 and W3 are buried, while the other members of this network are on the surface. At high temperatures, this network is likely to be unstable, further weakening the interactions between helices B and G, which may in turn increase the flexibility of the His116$^\beta$ side chain. This increased flexibility of the His116$^\beta$ side chain can affect the intersubunit contact with the carbonyl O of Ala14 of the α-chain, which is necessary for the stability. The structural alterations around the mutation site of HbE slightly expose the side chains of His117$^\beta$ and bury the negative charge of Glu22$^\beta$. These structural alterations, however, when coupled with the reorientation of Lys61$^\beta$ and the newly introduced positive charge of Lys26$^\beta$, create a patch of positive charge on the surface of HbE compared to that of HbA (Figure 3).

Table 4: Metal−Ligand Geometry and Interactions

	HbA_2^{FC}		HbE	
	α	δ	α	β^E
angle (deg)				
Fe−C−N	152	164	116	130
Fe−C−heme normal	1	1	2	2
distance (Å)				
Fe−C	2.20	2.35	2.32	2.27
Fe−Nε2 (His92)	2.17	2.14	2.13	2.13
C···Nε2 (His63)	2.97	3.13	2.74	2.99
N···Nε2 (His63)	3.03	3.20	3.16	3.06
C···Cδ2 (His63)	3.69	3.51	3.62	3.62
C···Cγ2 (Val67)	3.46	3.37	3.33	3.29
N···Cγ2 (Val67)	3.60	3.29	3.60	3.57
N···Cξ (Phe42)	3.65	3.50	–	–
N···Cδ2 (Leu28)	3.20	3.28	3.90	3.79

Heme Stereochemistry and Cyanide Binding. The heme stereochemistry and cyanide binding results presented here

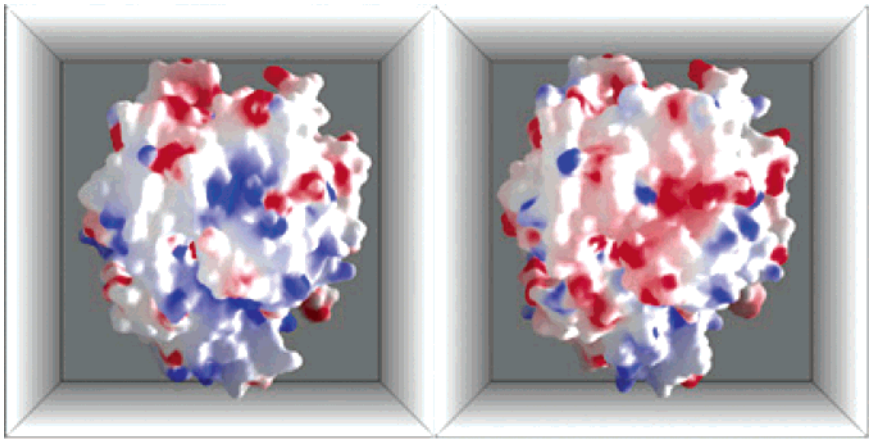

FIGURE 3: Surface representation, mapped with potential for (a) HbE and (b) HbA, that shows the cluster of positive charge at the mutation site of HbE compared to the corresponding site of HbA. Blue and red indicate positive and negative electrostatic potentials, respectively, at the molecular surface extending from +10 kT e^{-1} (dark blue) to −10 kT e^{-1} (dark red). This figure was generated with GRASP (*59*).

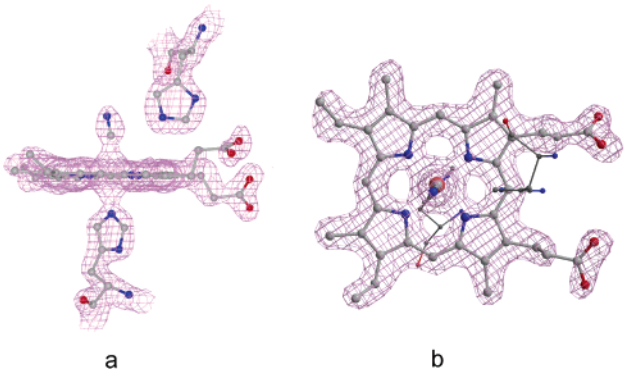

FIGURE 4: Electron density map ($2F_o - F_c$) around the heme group and the bound ligand of HbA_2, contoured at 1.2σ. The porphyrin ring, the CN ligand, and the distal and proximal histidines are shown in ball-and-stick form. Panel a shows the planarity of the heme group and the angular mode of binding of the CN ligand. Panel b is the top view of panel a showing the fitting of the porphyrin ring in the electron density. Here the proximal and distal histidines are shown as thin, dark-colored balls and sticks (without the electron density map) for clarity. This figure was generated with BOBSCRIPT (*60*) and RASTER3D (*58*).

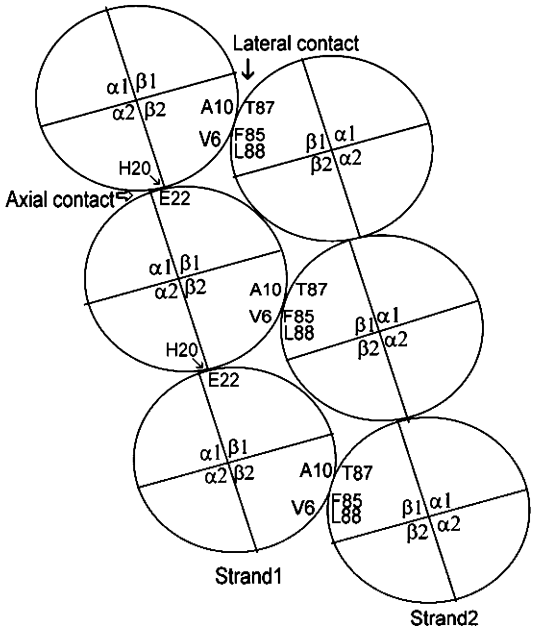

FIGURE 5: Schematic representation of sickling interactions as observed in the crystal structure of deoxy HbS (PDB entry 2HBS). Two types of contacts occur between HbS tetramers, incorporated in the polymer. Contacts along the long axis of the polymer are termed axial contacts, whereas the contacts that connect two strands are lateral contacts. Val6$^{\beta}$ plays a critical role in the lateral contact by interacting with hydrophobic residues Phe85$^{\beta}$ and Leu88$^{\beta}$. An important axial contact is the interaction of Glu22$^{\beta}$ with the imidazole group of His20$^{\alpha}$ on an adjacent tetramer.

from the structures of HbA_2 (1.88 and 2.2 Å) and HbE (1.74 Å) are important, particularly because very few crystal structures of cyanomet human hemoglobin are available in the Protein Data Bank. The geometries of binding of cyanide with heme groups of HbA_2^{FC} and HbA_2 are essentially the same, and hence, the details of ligand binding in HbA_2^{FC} and HbE only are given in Table 4. We compared our results with existing cyanomet structures such as human adult hemoglobin with tandem fusion of two α-chains (1ABY, 2.6 Å) as well as monomeric sperm whale myoglobin (1EBC, 1.8 Å), leghemoglobin (1LH3, 2.2 Å), and homotetrameric hemoglobin from *Urechis caupo* (1ITH, 2.5 Å).

The heme groups in both HbA_2 and HbE are remarkably planar. In each case, the iron atom is in the plane of the porphyrin ring and is bonded with the NE2 atom of the proximal histidine, His(F8)92 (with an average distance of 2.15 Å). OMIT maps ($2F_o - F_c$ and $F_o - F_c$) were calculated to confirm the planarity of the porphyrin ring where a strong electron density, attached with the heme iron, indicated the presence of a cyanide ligand (Figure 4). The cyanide ligands in all three structures are bound in a single well-defined conformation with full occupancies and low temperature factors (average values for HbA_2, HbA_2^{FC}, and HbE of 21.3, 18.2, and 24.2 Å^2, respectively).

The porphyrin ring of 1ABY is nonplanar, but it is almost planar for 1EBC, 1LH3, and 1ITH. The Fe−C−N angle of HbA_2 matches with those of 1EBC, 1LH3, and 1ITH, whereas the corresponding value of HbE matches that of 1ABY. Bolognesi *et al.* (35) reported that the Fe−C−N angles vary from 102° to 177° for different hemoglobins and concluded that the orientation of the diatomic cyanide ligand is dictated by the structural environment at the heme distal site. From the ligand−globin interactions (Table 4), we see that the contact involving Phe42 and CN is missing in HbE (in the case of both the α- and β-chains). Comparison of heme environment of HbA_2 and that of HbE show that there is a slight structural difference between them, which does not allow a near-linear mode of binding of the CN ligand in HbE. The Fe−C bond is relatively longer for HbA_2 and HbE (~2.25 Å) than for the others (1.83−2.08 Å). The other distances of the cyanide atoms from the neighboring residues are comparable.

Antisickling Effect of HbA_2. In sickle cell disease, the Val6$^{\beta}$ → Glu mutation (*36*, *37*) causes the formation of long polymers of deoxy HbS that distort normally pliable red blood cells. The crystal structure of deoxy HbS shows that the tetramers are assembled in double strands (Wishner−Love model) which are stabilized by axial contacts within each strand and lateral contacts between strands (Figure 5) that involve mutated Val6$^{\beta}$ (*38*, *39*). The primary inhibitory effect of HbF and HbA_2 on the polymerization of HbS (*7*, *40*) in the HbA_2/HbS and HbF/HbS mixtures is caused by the exclusion of asymmetrical hybrids $\alpha_2\beta^S\delta$ and $\alpha_2\beta^S\gamma$, respectively, as well as HbA_2 and HbF from the initiation of polymerization with HbS (*7*, *40*, *41*). Comparison of MGC values for naturally occurring Hb variants, like Lepore Hb, suggested that Gln87$^{\delta}$ and Ala22$^{\delta}$ of HbA_2 are potential sites for the inhibition of the polymerization of deoxy HbS (*8*). The antisickling capacity of a human β^A globin gene variant β^{A-T87Q} was assessed in transgenic mice, and the variant, extracted from their RBCs, was found to be almost as potent as an inhibitor as γ-globin *in vitro* (*42*). McCune *et al.* (*43*), from their modeling study, proposed that the larger side chain of Gln87 compared to that of Thr prevents the insertion of Val6$^{\beta S}$, but the crystal structure (2.05 Å, PDB entry 2HBS) of deoxy HbS, determined later, revealed that Thr87 of acceptor β_1^S is not a direct contact site for Val6; rather, Thr87 interacts with Ala13, Ala10, and Ser9 of donor β_2^S, whereas Val6 enters the hydrophobic pocket made by Phe85 and Leu88 of the acceptor β_1^S chain (*44*).

Since the inhibition of sickle cell polymerization by HbA_2 (and HbF) is primarily *in trans* to the Val6$^{\beta S}$ contact of the HbS polymer, the model of T state HbA_2 was superposed

Table 5: Comparison of Lateral Contacts As Seen in the Crystal Structure of 2HBS and in the Proposed Model of the HbA_2−HbS Hybrid

	contact in 2HBS (crystal structure)	contact in the HbA_2−HbS hybrid (model)
β_1^S Lys66 (O)−β_2^S Pro5 (CG)	3.61	4.14
β_1^S Gly69 (C)−β_2^S Pro5 (CG)	3.89	4.11
β_1^S Ala70 (N)−β_2^S Pro5 (CG)	3.83	3.91
β_1^S Ala70 (CB)−β_2^S Val6 (CG2)	3.83	3.70
β_1^S Asp73 (OD2)−β_2^S Thr4 (OG1)	3.11	2.66
β_1^S Asp73 (OD2)−β_2^S Val6 (CB)	3.10	3.52
β_1^S Asp79 (OD2)−α_2 Ser49 (CA)	3.46	3.76
β_1^S Asp79 (OD2)−α_2 His50 (N)	2.83	3.83
β_1^S Asn80 (CG)−α_2 His 50 (CD2)	3.65	3.89
β_1^S Gly83 (O)−β_2^S Pro125 (CG)	3.99	4.19
β_1^S Thr84 (O)−β_2^S Val6 (CG1)	3.62	3.41
β_1^S Phe85 (CE1)−β_2^S Val6 (CG2)	3.95	4.29
β_1^S Thr87 (CG2)−β_2^S Ala13 (CB)	3.65	–
β_1^S Thr87 (OG1)−β_2^S Ala10 (CA)	4.43	–
β_1^S Thr87 (CG2)−β_2^S Val126 (CG2)	5.98	–
β_1^S Leu88 (CD2)−β_2^S Ser9 (OG)	3.50	2.89
β_1^S Glu90 (OE2)−β_2^S Lys17 (NZ)	5.03	4.03
β_1^S Lys95 (NZ)−β_2^S Lys17 (NZ)	3.93	10.32

on one of the tetramers (chains A−D) of 2HBS such that it is in a position to accept $Val6^{\beta S}$ from the other tetramer of 2HBS (chain E−H). The combination of these two tetramers, one containing the superposed coordinates of T state HbA_2, acting as an acceptor for the donor $Val6^{\beta S}$, and the other tetramer of 2HBS (chains E−H), acting as the donor of $Val6^{\beta S}$, has been used as a model to understand the role of HbA_2 in antisickling. Lateral contacts, made by the donor β_2^S chain with the acceptor δ-chain of the T state HbA_2, are calculated and compared with the corresponding contacts, observed between donor β_2^S and acceptor β_1^S of 2HBS (Table 5). Most of the lateral contacts, observed in 2HBS, are retained, indicating the reliability of the T state model of HbA_2. However, a major difference is observed at $Gln87^{\delta}$ of HbA_2 where we have seen that the side chain of $Gln87^{\delta}$, beyond CB, follows the direction of the OG atom of $Thr87^{\beta}$, instead of CG2 (Figure 6). Hence the interactions, made by the CG2 atom of $Thr87^{\beta}$ with Ser9, Ala10, and Ala13 of β_2^S, for the formation of the HbS polymer are not possible with $Gln87^{\delta}$. Moreover, in this orientation, the OE1 and NE2 atoms of the longer side chain of $Gln87^{\delta}$ produce unfavorable contacts with the side chain of $Val126^{\beta}$ of β_2^S (Figure 6), further exacerbating the process of polymer formation.

Two other hemoglobin β87 variants support our observations. The compound heterozygosity of Hb D-Ibadan ($T87K^{\beta}$) and HbS does not result in sickling disorder (*45*), whereas in the HbS/Hb Quebec-Chori ($T87I^{\beta}$) mixture, Ile87 accelerates nucleation and polymerization (*46*). Our modeling studies suggest that in Hb Quebec-Chori ($T87I^{\beta}$), although Ile is slightly larger than Thr, it does not face any difficulty in maintaining hydrophobic contacts with Ser9, Ala10, and Ala13. In addition to that, its hydrophobic end can face the hydrophobic residues such as Pro125 and Val126 more favorably than ThrOG. In the case of Hb Ibadan, the situation is more or less like Gln87. It is difficult for the long side chain of Lys87 to face Ser9, Ala10, and Ala13 due to steric clash. On the other hand, if it follows the path of Thr87 OG, it will experience a steric hindrance from Val126 of β_2^S.

Model of δ_4 and Its Proposed Assembly Pathway. In case of α-thalassemia, excess β-type (β,γ,δ) globin chains self-aggregate to form homotetrameric hemoglobins with high oxygen affinity and no cooperativity. In this case, Hb Bart's

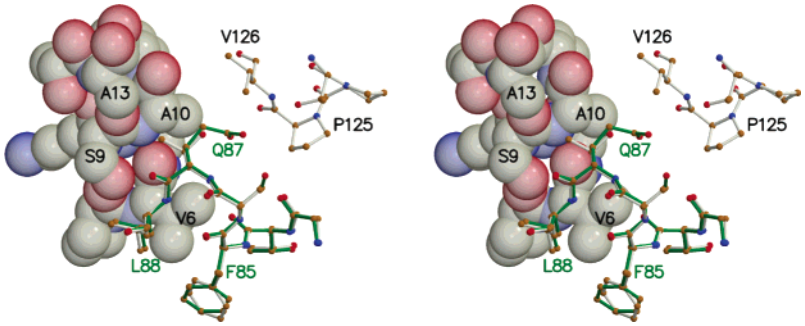

FIGURE 6: Antisickling effect of $Gln87^{\delta}$ of HbA_2. Val6−Ala13 of the donor β_2^S of the lateral contact site are shown as a space-filling model. The other part of the donor chain and the acceptor chain are shown as a ball-and-stick model (gray). The δ-chain of HbA_2 (green) is superposed on the acceptor β_1^S chain of HbS which shows that the side chain of $Gln87^{\delta}$ instead of following the direction of the CG atom of $Thr87^{\beta}$ follows OG and faces $Val126$ of β_2^S. This figure was generated using MOLSCRIPT (*57*) and RASTER3D (*58*).

Table 6: Comparison of Intersubunit Contacts at the $\delta_1\delta_2$ Interface of Hb δ_4 with the Corresponding Contacts of CN-Bound HbA_2 (at the $\alpha_1\delta_1$ Interface) and of CO-β_4 (at the $\beta_1\beta_2$ Interface)

CN-HbA_2 $\delta_1(\delta_2)$ residue	CN-HbA_2 $\alpha_1(\alpha_2)$ residue	distance (Å[a]	δ_4 model $\delta_2(\delta_4)$ residue	δ_4 model $\delta_1(\delta_3)$	distance (Å)
$Arg30^{\delta}$ NH2	$His122^{\alpha}$ ND1	3.18 (2.75)[a]	$Arg30^{\delta}$ NH1	$Gln127^{\delta}$ OE1	2.73 (2.78)[b]
$Arg30^{\delta}$ NH1	$Phe117^{\alpha}$ O	2.87 (3.08)[a]	$Arg30^{\delta}$ NH1	$Phe122^{\delta}$ O	3.18 (2.81)[b]
$Asn108^{\delta}$ O	$His103^{\alpha}$ NE2	3.46 (3.08)[a]			
			$Asp52^{\delta}$ OD2	$Gln125^{\delta}$ NE2	3.09
$Arg116^{\delta}$ NH1	$Pro114^{\alpha}$ O	3.60 (2.89)[a]	$Arg116^{\delta}$ NH1	$Gly119^{\delta}$ O	3.43 (2.73)[b]
			$Arg116^{\delta}$ NH1	$Ala120^{\delta}$ N	2.78
			$Gly119^{\delta}$ O	$Arg116^{\delta}$ NH1	2.95 (3.12)[b]
			$Ala120^{\delta}$ N	$Arg116^{\delta}$ NH1	2.62
$Phe122^{\delta}$ O	$Arg31^{\alpha}$ NH1	2.58 (2.7)[a]	$Phe122^{\delta}$ O	$Arg30^{\delta}$ NH1	3.43 (2.75)[b]
			$Gln125^{\delta}$ NE2	$Asp52^{\delta}$ OD2	3.55
$Gln127^{\delta}$ OE1	$Arg31^{\alpha}$ NH2	2.96 (2.78)[a]	$Gln127^{\delta}$ OE1	$Arg30^{\delta}$ NH1	2.72 (2.79)[b]
$Gln131^{\delta}$ OE1	$His103^{\alpha}$ CE1	2.79 (3.08)[a]			

[a] Values in parentheses are the corresponding contact distances for HbA. [b] Values in parentheses are the corresponding contact distances for CO-β_4.

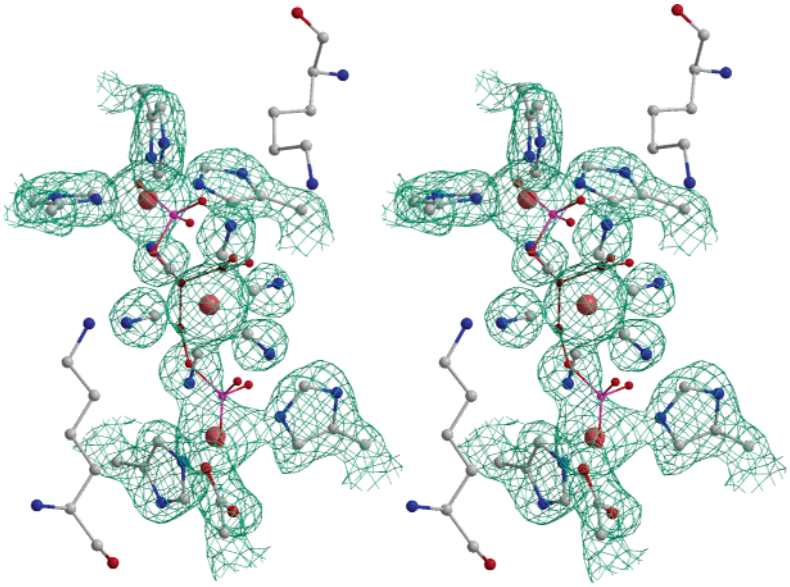

FIGURE 7: Stereoscopic representation of the mode of ferrocyanide binding in HbA_2^{FC}. Three iron atoms (Fe1−Fe3) from the top (rust) and their attached ligands (atom color) are shown in a ball-and-stick model. His143, His146 of δ_1, and His143 of δ_2 are coordinated (clockwise, left to right) with Fe1, whereas His146 of δ_2 and Asp47 and His50 of a symmetry-related α_2 chain are coordinated (counterclockwise, left to right) with Fe3. A $2F_o - F_c$ electron density map, contoured at 1.2σ, is also overlaid on these atoms (except Lys82 for clarity). The coordinates of the DPG molecule (red ball-and-stick model), obtained from 1B86, are superposed on the iron atoms which shows that the total length covered by the iron atoms matches the length of DPG. This figure was generated with MOLSCRIPT (*57*) and RASTER3D (*58*).

(γ_4) is produced in infancy and HbH (β_4) in adulthood (*47*), whereas in "rare HbH disease", a homotetramer like δ_4 (*48*) is produced. The structural and functional features of β_4 (*30*, *31*, *47*) and γ_4 (*32*) have been investigated in detail, but very little is known about the structural and functional properties of δ_4. It is reported that in contrast to the $4\beta \leftrightarrow \beta_4$ pathway of HbH, the tetramerization of γ_4 proceeds through the formation of predominant amounts of γ_2 (*49*). The structure of δ_4, modeled here, has been analyzed in terms of intersubunit contacts and compared with the corresponding interfaces of β_4, HbA_2, and HbA. Analysis of the δ_4 model shows that four (of 10) δ-chain mutations of Arg116, Asn117, Gln125, and Met126 are present near the $\delta_1\delta_2$ interface (corresponding to the $\beta_1\beta_2$ interface of β_4), but none of the mutations is present near the $\delta_1\delta_4$ interface (corresponding to the $\beta_1\beta_4$ interface). Analyses of the interactions at the $\delta_1\delta_2$ interface of δ_4 indicate that the mutations of $Arg116^{\delta}$ and $Gln125^{\delta}$ can form extra hydrogen bonds at the $\delta_1\delta_2$ interface (Table 6). The $Pro125^{\beta} \rightarrow Gln125^{\delta}$ mutation of δ_1 can form new hydrogen bonds with Asp52 OD2 of δ_2; likewise, Gln125 of δ_2 forms hydrogen bonds with Asp52 OD2 of δ_1. In β_4, His116 of β_1 forms a hydrogen bond with the carbonyl O of Gly119 of the neighboring chain at the $\beta_1\beta_2$ interface. In δ_4, $Arg116^{\delta}$ NH1 of δ_1, apart from maintaining the above interaction, forms an extra hydrogen bond with Ala120 N of δ_2. A similar interaction is also possible for Arg116 of δ_2 with the corresponding δ_1 residue. Therefore, δ_4 gains four extra hydrogen bonds at the $\delta_1\delta_2$ interface, compared to β_4.

Borgstahl *et al*. (*30*) showed that the $\beta_1\beta_2$ interface in CO-β_4 is less stable, compared to the corresponding $\alpha_1\beta_1$ interface of HbA, while the $\beta_1\beta_4$ interface is more stable compared to the corresponding $\alpha_1\beta_2$ interface. This reversal in subunit interface stabilities is the dominant structural reason for the different pathways of formation of homotetrameric and heterotetrameric assembly. Any mutation that strengthens the $\beta_1\beta_2$ interface or weakens the $\beta_1\beta_4$ interface of a β_4-type homotetramer should alter the monomer tetramer assembly mechanism to one in which a significant amount of dimer is observed. Mutagenesis studies on β-type globin chains suggest that residue 116 (G18) contributes significantly to the differences between the pathway of heterotetramer formation (*49*) and the pathway of homotetramer formation (*50*). Ile116 of the γ-chain is responsible for stable γ_2 dimer formation and follows the $4\gamma \leftrightarrow \gamma_2 \leftrightarrow \gamma_4$ assembly pathway, whereas the $Ile116^{\gamma} \rightarrow$ His mutation promotes the dissociation of γ_4 to monomers through a $4\gamma \leftrightarrow \gamma_4$ assembly pathway. It was suggested that the burial of hydrophobic $Ile116^{\gamma}$ strengthens the $\gamma_1\gamma_2$ interface, compared to the $\beta_1\beta_2$ interface, which is reflected in the $4\gamma \leftrightarrow \gamma_2 \leftrightarrow \gamma_4$ assembly pathway. Superpositioning of δ_4 on γ_4 shows that the hydrophobic part of $Arg116^{\delta}$ mimics the hydrophobic interactions, made by $Ile116^{\gamma}$ with Ala115 and Phe122 of the neighboring globin chain at the $\delta_1\delta_2$ interface, while the polar NH1 atom of $Arg116^{\delta}$ forms two extra hydrogen bonds, compared to the corresponding interface of β_4. In the cases where the $\beta_1\beta_4$ interactions are weaker, tetramerization also proceeds through dimer formation, like in Hb-Kempsey ($Asp99^{\beta} \rightarrow$ Asn) where the salt bridge between Arg40 and Asp99 at the $\beta_1\beta_4$ ($\alpha_1\beta_2$) interface is absent. Since the interactions at the $\delta_1\delta_4$ interface of δ_4 remain the same as those at the $\beta_1\beta_4$ interface of CO-β_4 but the $\delta_1\delta_2$ interface acquires additional stability through the extra interactions, made by $Arg116^{\delta}$ and $Gln125^{\delta}$ (Table 6), compared to β_4, it is expected that formation of δ_4 follows a $4\delta \leftrightarrow \delta_2 \leftrightarrow \delta_4$ assembly pathway compared to the $4\beta \leftrightarrow \beta_4$ pathway in β_4.

Identification of the Ferrocyanide Binding Site in Hemoglobin. The ferrocyanide anion, formed during the preparation of methemoglobin using $K_3[Fe(CN)_6]$, binds hemoglobin probably at the same site where DPG binds (*16*). However, the binding of ferrocyanide to methemoglobin is abolished in the presence of inositol hexaphosphate (IHP), indicating

that IHP competes for the ferrocyanide binding site (*16*). Crystallographic studies showed that the binding site for DPG is constituted by multiple positively charged residues (*51*) from each β-chain of T state hemoglobin: α-amino group, His2, Lys82, and His143. During the refinement of HbA_2^{FC} with 1.88 Å data, we have found three strong positive peaks near C-terminal residues His143 (involved in DPG binding) and His146 of each δ-chain, which were assigned as iron atoms (named Fe1−Fe3). Among them, Fe1 and Fe3 have tetrahedral coordination, whereas Fe2 is centrally located and is octahedrally coordinated (Figure 7) with six CN ligands (average Fe−C distance of 2.0 Å). Fe2 connects Fe1 and Fe3 through the N atoms of its bridging CN groups (average Fe−N distance of 1.9 Å). Moreover, positively charged Lys82 residues of both the δ-chains, implicated in DPG binding, were found to form hydrogen bonds and/or charge interactions with two other cyanide groups coordinated to Fe2. In accordance with the previous report that $K_4[Fe(CN)_6]$ binds to methemoglobin (*16*), the octahedrally coordinated central moiety (Fe2 with six attached ligands) was identified as $Fe(CN)_6^{4-}$ where the iron atom is in +II oxidation state. In presence of strong cyanide ligands, Fe2 iron is likely to be in a low-spin state with a high crystal field stabilization energy (CFSE) of −24Dq+2P. Apart from the bridging CN ligand, Fe1 fulfills its tetrahedral coordination with His146 of δ_1 and His143 and His146 of the δ_2 globin chains. On the other hand, along with His143 of δ_1, Fe3 fulfills its coordination with two symmetry-related residues, Asp47 and His50 of the α_2 globin chain. The oxidation states of tetrahedrally coordinated Fe1 and Fe3 are also kept as +II in our crystal structure. The *B*-factors of these three iron atoms (average value of 16 $Å^2$) and six cyanide ligands (average value of 19 $Å^2$) are considerably low, indicating their tight binding, as reported by Brunori *et al.* (*52*).

When the coordinates of DPG were optimally superposed on the Fe1−Fe2−Fe3 motif, it showed that the distance covered by these three iron atoms matches the length of DPG (Figure 7). Moreover, the geometry of the terminal iron atoms is similar to that of the terminal phosphate groups of DPG, whereas the bridging ligands, connecting Fe2 with Fe1 and Fe3, correspond to the positions of O_2 and O_5 of DPG. One ferrocyanide anion alone does not match DPG, either in length or in geometry, but the assembly of ferrocyanide anion and the two tetrahedral irons is such that it can mimic the structure of DPG. The crystal structure of IHP-bound hemoglobin at 1.5 Å (PDB entry 1THB) (*53*) is also compared with that of HbA_2^{FC}. The distance between the phosphate groups of IHP that bind $His2^{\beta}$ and $His143^{\beta}$ is comparable with the distance between the two tetrahedral iron atoms, Fe1 and Fe3 of HbA_2^{FC}.

DPG and IHP bind positively charged terminal histidyl residues of T state hemoglobin. In this structural study, we have seen that although HbA_2 binds ferrocyanide anion in the R2 state, it uses some of the DPG binding histidyl residues. In the structure of HbA_2^{FC}, these histidyl residues bind with terminal tetrahedral iron atoms Fe1 and Fe3 at pH 8.5. The analysis of the binding of these histidyl residues with positively charged Fe1 and Fe3 indicates that a basic pH is required where the histidyl residues become deprotonated and can facilitate binding with positively charged Fe1 and Fe3. To study further the effect of pH on the binding of ferrocyanide anion with hemoglobin, oxy-HbA equilibrated

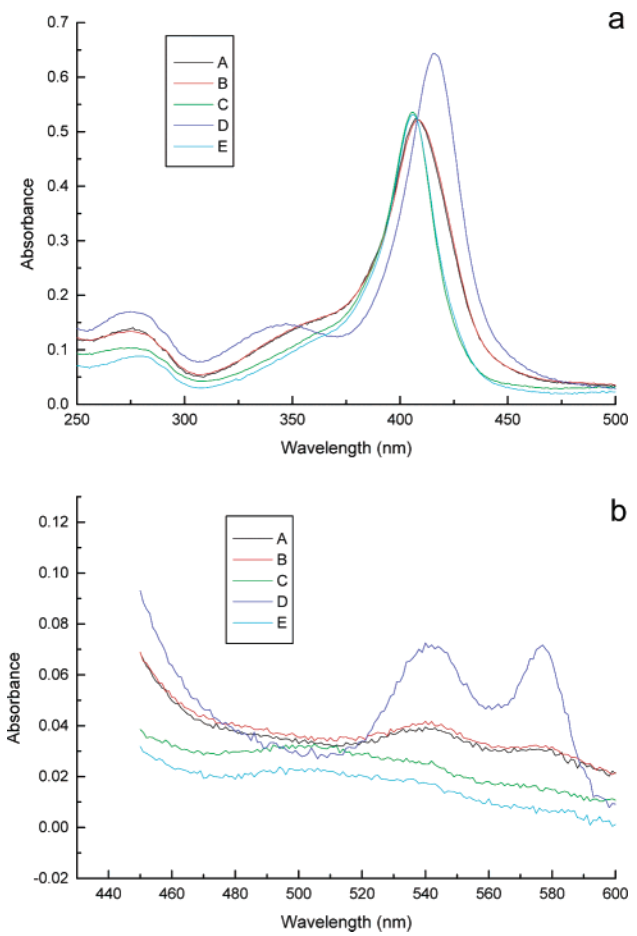

FIGURE 8: UV−vis spectra for (A) crystals of HbA_2^{FC} dissolved in 50 mM Tris (pH 8.5), (B) hemoglobin fraction collected at pH 8.5, (C) hemoglobin fractions collected at pH 5.5, (D) oxyhemoglobin, and (E) hemoglobin fraction collected at pH 6.2. The spectra are presented for the Soret region (a) and the visible region (b).

at different pH values was treated with ferricyanide (see Materials and Methods), and the shift in the absorption maximum (λ_{max}) and the total OD_{415} were checked. Oxy-HbA samples, taken for experiments, showed peaks at 415 nm in the Soret region and 540 and 576 nm in the visible region. Samples treated with ferricyanide at pH 5.5 and 6.2 consistently produced a λ_{max} value of 406 nm, whereas for pH 8.5, this λ_{max} value was shifted to 408 nm (Figure 8a). Interestingly, the crystals of ferrocyanide-bound HbA_2 (HbA_2^{FC}) dissolved in 50 mM Tris-HCl (pH 8.5) also showed a λ_{max} of 408 nm which matches exactly that of the ferricyanide-treated sample of HbA at pH 8.5 (Figure 8a). However, the spectra, shown in Figure 8b, correspond well with the reported differences between methemoglobin at different pH values with the oxyhemoglobin in the visible region (*54*). All these measurements were carried out three times for a given pH, and the results were consistent. Calculations of the total OD_{415} for the hemoglobin fractions eluted from the G-25 column at different pH values showed that the total OD_{415} value is minimal (11.3) at pH 5.5 and maximal (17.5) at pH 8.5, whereas this value is intermediate (13.4) at pH 6.2. This increment of total OD_{415} with pH cannot be attributed to only the change in the molar extinction coefficient at different pH values in Soret region. Hence, we suggest that this increment of OD_{415} with pH may be a result of ferrocyanide binding with hemoglobin which

is facilitated at basic pH, as indicated by the structure of HbA_2^{FC}. Since the residues of HbA_2, involved in ferrocyanide binding, are the same as those of HbA, one may probably expect that the binding sites for ferrocyanide in HbA and HbA_2 are the same.

Various kinetic experiments have conclusively shown that electron transfer can take place over a large distance in the protein interiors of modified proteins or protein complexes which involve protein-bound metal ions that are separated by relatively large distances as observed in various heme proteins such as ruthenium derivatives of myoglobin where the closest edge−edge distance between heme and Ru-bound His is ∼20 Å (*55*). In *Scapharca* dimeric hemoglobin, it was also observed that ferrocyanide anion binds with the oxidized form of the protein and the combination acts as the intramolecular redox couple (*56*). In this case, the distance between the bound ferrocyanide anion and the heme iron of the same subunit was ∼15 Å, a distance which allowed for efficient intramolecular electron transfer. In HbA_2^{FC}, we have seen that the distance of Fe2 from the heme edge of δ-chains is ∼18 Å, whereas the distances of histidyl residues bound from their closest heme edge to Fe1 or Fe3 are ∼12 Å. Therefore, the possibility of intramolecular electron transfer between bound ferrocyanide and heme iron(III) of methemoglobin cannot be ruled out.

SUPPORTING INFORMATION AVAILABLE

Two $2F_o - F_c$ electron density maps around δ-chain residues of HbA_2 and stereoscopic representation of the mode of ferrocyanide binding in HbA_2^{FC}. This material is available free of charge via the Internet at http://pubs.acs.org.

REFERENCES

1. Coleman, M. B., Adams, J. G., III, Plonczynski, M. W., Harrell, A. H., Walker, A. M., Fairbanks, V., and Steinberg, M. H. (1992) β-Thalassemia intermedia with exceptionally high hemoglobin A_2: relationship to mutations in the β-gene promoter, *Am. J. Med. Sci. 304* (2), 73−78.
2. Huisman, T. H. J., Dozy, A. M., Nechtman, C., and Thompson, R. B. (1962) Oxygen Equilibrium of Hemoglobin A_2 and Its Variant Hemoglobin A_2 (or B_2'), *Nature 195*, 1109−1110.
3. DeBruin, S. H., and Jansen, L. H. M. (1973) Comparison of the oxygen and proton binding behavior of human hemoglobin A and A_2, *Biochim. Biophys. Acta. 295*, 490−494.
4. Inagaki, K., Inagaki, J., Dumoulin, A., Padovan, J. C., Chait, B. T., Popowicz, A., Manning, L. R., and Manning, J. M. (2000) Expression and Properties of Recombinant HbA2 ($\alpha 2\delta 2$) and Hybrids Containing δ-β sequences, *J. Protein Chem. 19* (8), 649−662.
5. Russu, I. M., Lin, A. K., Ferro-Dosch, S., and Ho, C. (1984) A proton nuclear magnetic resonance investigation of human hemoglobin A_2, *Biochim. Biophys. Acta 785* (3), 123−131.
6. Perutz, M. F., and Raidt, H. (1975) Stereochemical basis of heat stability in bacterial ferredoxins and in haemoglobin A2, *Nature 255*, 256−259.
7. Nagel, R. L., Bookchin, R. M., Johnson, J., Labie, D., Wajcman, H., Isaac-Sodeye, W. A., Honig, G. R., Schiliro, G., Crookston, J. H., and Matsutomo, K. (1979) Structural bases of the inhibitory effects of hemoglobin F and hemoglobin A2 on the polymerization of hemoglobin S, *Proc. Natl. Acad. Sci. U.S.A. 76* (2), 670−672.
8. Adachi, K., Pang, J., Reddy, L. R., Bradley, L. E., Chen, Q., Trifillis, P., Schwartz, E., and Surrey, S. (1996) Polymerization of three hemoglobin A2 variants containing Val6 and inhibition of hemoglobin S polymerization by hemoglobin A2, *J. Biol. Chem. 271* (40), 24557−24563.
9. Orkin, S. H., Kazazian, H. H., Jr., Antonarakis, S. E., Ostrer, H., Goff, S. C., and Sexton, J. P. (1982) Abnormal RNA processing due to the exon mutation of β E-globin gene, *Nature 300* (5894), 768−769.
10. Shirohzu, H., Yamaza, H., and Fukumaki, Y. (2000) Repression of aberrant splicing in human β-globin pre-mRNA with HbE mutation by antisense oligoribonucleotide or splicing factor SF2/ASF, *Int. J. Hematol. 72* (1), 28−33.
11. Weatherall, D., and Clegg, J. B. (1981) *The Thalassaemia Syndromes*, Blackwell, Oxford, U.K.
12. Weatherall, D., and Clegg, J. (1996) Thalassemia: a global public health problem, *Nat. Med. 3*, 847−849.
13. Hutagalung, R., Wilairatana, P., Looareesuwan, S., Brittenham, G. M., and Gordeuk, V. R. (2000) Influence of hemoglobin E trait on the antimalarial effect of artemisinin derivatives, *J. Infect. Dis. 181*, 1513−1516.
14. Rees, D. C., Clegg, J. B., and Weatherall, D. J. (1998) Is Hemoglobin Instability Important in the Interaction Between Hemoglobin E and β Thalassemia? *Blood 92* (6), 2141−2146.
15. Pscheidt, S., Pereima, M. L., Roberge, M. B., Rotolo, M. A. S., Genovez, G., and Zunino, J. N. (2003) Köln's unstable hemoglobin: case report and literature review, *J. Bras. Patol. Med. Lab. 39* (1), 37−40.
16. Kilmartin, J. V. (1973) The interaction of inositol hexaphosphate with methaemoglobin, *Biochem. J. 133* (4), 725−733.
17. Hoffman, B. M., and Bull, C. (1976) Linearity of the hemoglobin oxidation bohr effect, *Proc. Nat. Acad. Sci. U.S.A. 73* (3), 800−803.
18. Dasgupta, J., Sen, U., Choudhury, D., Datta, P., Chakrabarti, A., Chakrabarty, S. B., Chakrabarty, A., and Dattagupta, J. K. (2003) Crystallization and preliminary X-ray structural studies of hemoglobin A2 and hemoglobin E, isolated from the blood samples of β-thalassemic patients, *Biochem. Biophys. Res. Commun. 303* (2), 619−623.
19. Clegg, J. B., and Weatherall, D. J. (1981) Screening Procedures for quantitative Abnormalities in Hemoglobin Synthesis, *Methods Enzymol. 76*, 749−760.
20. Otwinowski, Z., and Minor, W. (1997) Processing of X-ray diffraction data collected in oscillation mode, *Methods Enzymol. 276*, 307−326.
21. Collaborative Computational Project, Number 4 (1994) The CCP4 suite: Programs for protein crystallography, *Acta Crystallogr. D50*, 760−763.
22. Fermi, G., Perutz, M. F., Shaanan, B., and Fourme, R. (1984) The crystal structure of human deoxyhaemoglobin at 1.74 Å resolution, *J. Mol. Biol. 175*, 159−174.
23. Shaanan, B. (1983) Structure of human oxyhaemoglobin at 2.1 Å resolution, *J. Mol. Biol. 171*, 31−59.
24. Silva, M. M., Rogers, P. H., and Arnone, A. (1992) A third quaternary structure of human hemoglobin A at 1.7 Å resolution, *J. Biol. Chem. 267*, 17248−17256.
25. Brünger, A. T. (1992) Free R-value: A novel statistical quantity for assessing the accuracy of crystal structures, *Nature 355*, 472−475.
26. Jones, T. A., Zou, J. Y., Cowan, S. W., and Kjeldgaard, M. (1991) Improved methods for building protein models in electron density maps and the location of errors in these models, *Acta Crystallogr. A47*, 110−119.
27. Brünger, A. T., Adams, P. D., Clore, G. M., DeLano, W. L., Gros, P., Grosse-Kunstleve, R. W., Jiang, J.-S., Kuszewski, J., Nilges, M., Pannu, N. S., Read, R. J., Rice, L. M., Simonson, T., and Warren, G. L. (1998) Crystallography & NMR system: A new software suit for macromolecular structure determination, *Acta Crystallogr. D54*, 905−921.
28. Perutz, M. F. (1972) Nature of haem-haem interaction, *Nature 237* (5357), 495−499.
29. Baldwin, J., and Chothia, C. (1979) Haemoglobin: the structural changes related to ligand binding and its allosteric mechanism, *J. Mol. Biol. 129* (2), 175−220.
30. Borgstahl, G. E. O., Rogers, P. H., and Arnone, A. (1994) The 1.8 Å structure of carbonmonoxy-β4 hemoglobin. Analysis of a homotetramer with the R quaternary structure of liganded $\alpha_2\beta_2$ hemoglobin, *J. Mol. Biol. 236* (3), 817−830.
31. Borgstahl, G. E. O., Rogers, P. H., and Arnone, A. (1994) The 1.9 Å structure of deoxy β4 hemoglobin. Analysis of the partitioning of quaternary-associated and ligand-induced changes in tertiary structure, *J. Mol. Biol. 236* (3), 831−843.
32. Kidd, R. D., Baker, H. M., Mathews, A. J., Brittain, T., and Baker, E. N. (2001) Oligomerization and ligand binding in a homotetrameric hemoglobin: two high-resolution crystal structures of hemoglobin Bart's (γ_4), a marker for α-thalassemia, *Protein Sci. 10*, 1739−1749.

33. Laskowski, R. A., MacArthur, M. W., Moss, D. S., and Thornton, J. M. (1993) Main-chain bond lengths and bond angles in protein structures, *J. Appl. Crystallogr. 26*, 283−291.
34. Kinderlerer, J., Lehmann, H., and Tipton, K. F. (1973) The thermal denaturation of human oxyhemoglobins A, A_2, C and S, *Biochem. J. 135*, 805−814.
35. Bolognesi, M., Rosano, C., Losso, R., Borassi, A., Rizzi, M., Wittenberg, J. B., Boffi, A., and Ascenzi, P. (1999) Cyanide binding to *Lucina pectinata* Hemoglobin I and to Sperm Whale Myoglobin: An X-ray crystallographic study, *Biophys. J. 77*, 1093−1099.
36. Ingram, V. M. (1956) A specific chemical difference between the globins of normal human and sickle-cell anaemia haemoglobin, *Nature 178*, 792−794.
37. Ingram, V. M. (1957) Gene mutations in human haemoglobin: the chemical difference between normal and sickle cell haemoglobin, *Nature 180*, 326−328.
38. Wishner, B. C., Ward, K. B., Lattman, E. E., and Love, W. E. (1975) Crystal structure of sickle-cell deoxyhemoglobin at 5 Å resolution, *J. Mol. Biol. 98*, 179−194.
39. Wishner, B. C., Hanson, J. C., Ringle, W. M., and Love, W. E. (1976) in *Proceedings of the Symposium on Molecular and Cellular Aspects of Sickle Cell Disease* (Hercules, J. I., Cottam, G. L., Waterman, M. R., and Schechter, A. N., Eds.) pp 1−31, DHEW Publ. No. (NIH) 76-1003, Bethesda, MD.
40. Bookchin, R. M., Nagel, R. L., and Balazs, T. (1975) Role of hybrid tetramer formation in gelation of haemoglobin S, *Nature 256* (5519), 667−668.
41. Adachi, K., Kim, J., Asakura, T., and Schwartz, E. (1990) Characterization of two types of fetal hemoglobin: $\alpha_{2G}\gamma_2$ and $\alpha_{2A}\gamma_2$, *Blood 75* (10), 2070−2075.
42. Pawliuk, R., Westerman, K. A., Fabry, M. E., Payen, E., Tighe, R., Bouhassira, E. E., Acharya, S. A., Ellis, J., London, I. M., Eaves, C. J., Humphries, R. K., Beuzard, Y., Nagel, R. L., and Leboulch, P. (2001) Correction of sickle cell disease in transgenic mouse models by gene therapy, *Science 294* (5550), 2368−2371.
43. McCune, S. L., Reilly, M. P., Chomo, M. J., Asakura, T., and Townes, T. M. (1994) Recombinant human hemoglobins designed for gene therapy of sickle cell disease, *Proc. Natl. Acad. Sci. U.S.A. 91* (21), 9852−9856.
44. Harrington, D. J., Adachi, K., and Royer, W. E., Jr. (1997) The high-resolution crystal structure of deoxyhemoglobin S, *J. Mol. Biol. 272*, 398−407.
45. Redding-Lallinger, R., Tankut, G., Holley, L., Wright, F., Kutlar, A., and Kutlar, F. (2002) Molecular characterization of Hb D-Ibadan [β87(F3)Thr → Lys] in combination with Hb S [β6-(A3)Glu → Val] and with β+-Thalassemia: report of two cases, *Hemoglobin 26* (2), 129−134.
46. Witkowska, H. E., Lubin, B. H., Beuzard, Y., Baruchel, S., Esseltine, D. W., Vichinsky, E. P., Kleman, K. M., Bardakdjian-Michau, J., Pinkoski, L., and Cahn, S. (1991) Sickle cell disease in a patient with sickle cell trait and compound heterozygosity for hemoglobin S and hemoglobin Quebec-Chori, *N. Engl. J. Med. 325* (16), 1150−1154.
47. Rigas, D. A., Koler, R. D., and Osgood, E. E. (1956) Hemoglobin H; clinical, laboratory, and genetic studies of a family with a previously undescribed hemoglobin, *J. Lab. Clin. Med. 47*, 51−64.
48. Dance, N., and Huehns, E. R. (1962) A haemoglobin containing only delta chains, *Biochem. Biophys. Res. Commun. 7*, 444−447.
49. Adachi, K., Zhao, Y., Yamaguchi, T., and Surrey, S. (2000) Assembly of γ- with α-globin chains to form human fetal hemoglobin in vitro and in vivo, *J. Biol. Chem. 275*, 12424−12429.
50. Adachi, K., Yang, Y., Lakka, V., Wehrli, S., Reddy, K. S., and Surry, S. (2003) Significance of β116 His (G18) at $\alpha 1\beta 1$ contact sites for $\alpha\beta$ and autoxidation of hemoglobin, *Biochemistry 42*, 10252−10259.
51. Richard, V., Dodson, G. G., and Mauguen, Y. (1993) Human deoxyhaemoglobin-2,3-diphosphoglycerate complex low-salt structure at 2.5 Å resolution, *J. Mol. Biol. 233*, 270−274.
52. Brunori, M., Wyman, J., Antonini, E., and Rossi-Fanelli, A. (1965) Studies on the oxidation−reduction potentials of heme proteins. V. The oxidation Bohr effect in normal human hemoglobin and human hemoglobin digested with carbopeptidase A, *J. Biol. Chem. 240*, 3317−3324.
53. Waller, D. A., and Liddington, R. C. (1990) Refinement of a partially oxygenated T state human haemoglobin at 1.5 Å resolution, *Acta Crystallogr. B46*, 409−418.
54. Iorio, E. E. Di. (1981) Preparation of Derivatives of Ferrous and Ferric Hemoglobin, *Methods Enzymol. 76*, 57−72.
55. Mayo, S. L., Ellis, W. R., Jr., Crutchley, R. J., and Gray, H. B. (1986) Long-range electron transfer in heme proteins, *Science 23*, 949−952.
56. Colotti, G., Verzili, D., Boffi, A., and Chiancone, E. (1994) Identification of the site of ferrocyanide binding involved in the intramolecular electron transfer process to oxidized heme in *Scapharca* dimeric hemoglobin, *Arch. Biochem. Biophys. 311* (1), 103−106.
57. Kraulis, P. J. (1991) MOLSCRIPT: A program to produce both detailed and schematic plots of protein structures, *J. Appl. Crystallogr. 24*, 946−950.
58. Merritt, E. A., and Bacon, D. J. (1997) Raster3D: Photorealistic Molecular Graphics, *Methods Enzymol. 277*, 505−524.
59. Nicholls, A., Sharp, K., and Honig, B. (1991) Protein folding and association: insights from the interfacial and thermodynamic properties of hydrocarbons, *Proteins 11*, 281−296.
60. Esnouf, R. M. (1997) An extensively modified version of MolScript that includes greatly enhanced coloring capabilities, *J. Mol. Graphics Modell. 15*, 132−134.

BI048903I